Rapid Communications

Weakly coupled alternating $S = \frac{1}{2}$ chains in the distorted honeycomb lattice compound $Na_2Cu_2TeO_6$

Shang Gao,[1,2] Ling-Fang Lin,[3] Andrew F. May,[1] Binod K. Rai,[1] Qiang Zhang,[2] Elbio Dagotto,[1,3] Andrew D. Christianson,[1] and Matthew B. Stone[2]

[1]*Materials Science & Technology Division, Oak Ridge National Laboratory, Oak Ridge, Tennessee 37831, USA*
[2]*Neutron Scattering Division, Oak Ridge National Laboratory, Oak Ridge, Tennessee 37831, USA*
[3]*Department of Physics and Astronomy, University of Tennessee, Knoxville, Tennessee 37996, USA*

(Received 3 October 2020; accepted 17 November 2020; published 2 December 2020)

Spin-$\frac{1}{2}$ chains with alternating antiferromagnetic (AF) and ferromagnetic (FM) couplings exhibit quantum entanglement as the integer-spin Haldane chains and might be similarly utilized for quantum computations. Such alternating AF-FM chains have been proposed to be realized in the distorted honeycomb lattice compound $Na_2Cu_2TeO_6$, but to confirm this picture a comprehensive understanding of the exchange interactions including terms outside of the idealized model is required. Here, we employ neutron scattering to study the spin dynamics in $Na_2Cu_2TeO_6$ and accurately determine the coupling strengths through the random phase approximation and density functional theory approaches. We find the AF and FM intrachain couplings are the dominant terms in the spin Hamiltonian, while the interchain couplings are AF but perturbative. This hierarchy in the coupling strengths and the alternating signs of the intrachain couplings can be understood through their different exchange paths. Our results establish $Na_2Cu_2TeO_6$ as a weakly coupled alternating AF-FM chain compound and reveal the robustness of the gapped ground state in alternating chains under weak interchain couplings.

DOI: 10.1103/PhysRevB.102.220402

Introduction. Spin-$\frac{1}{2}$ chains with alternating antiferromagnetic (AF) and ferromagnetic (FM) couplings are known to exhibit gapped excitations and exponentially decaying correlations [1,2], which are different from those of the spin-$\frac{1}{2}$ Bethe chains with uniform couplings [3] but more similar to the spectrum of integer-spin Haldane chains [4,5]. Assuming alternating couplings of J_1 (AF) and $J_2 = \beta J_1$ ($\beta < 1$), the Hamiltonian of an alternating chain can be written as $\mathcal{H} = \sum_j J_1 \boldsymbol{S}_{2j-1} \cdot \boldsymbol{S}_{2j} + \sum_j J_2 \boldsymbol{S}_{2j} \cdot \boldsymbol{S}_{2j+1}$. In the special case of $\beta = 0$, an alternating chain can be viewed as disconnected spin dimers, and the local singlet-triplet (triplon) excitations over the dimers account for the excitation gap in the spectrum. Nonzero J_2 couplings will introduce dispersion for the triplon excitations. At $\beta = 1$, one recovers the gapless character of a Bethe chain. In the whole range of $-\infty < \beta < 1$, theoretical calculations have revealed a hidden string order that is protected by the $Z_2 \times Z_2$ global rotation symmetry [6,7], showing that the gapped ground state of alternating chains is a symmetry-protected topological state of the same type as that of Haldane chains [8]. Considering the prospect of Haldane chains as the resource ground state for measurement-based quantum computation [9], the additional degrees of freedom in $S = \frac{1}{2}$ alternating chains may be important to explore further flexibility in qubit operations.

Experimental realizations of alternating AF-FM chains are limited to a few compounds, including $CuNb_2O_6$ [10], $DMACuCl_3$ [11], $Na_3Cu_2SbO_6$ [12], and $BaCu_2V_2O_8$ [13], where the exchange couplings have been accurately determined through neutron scattering. Recently, a new candidate compound, $Na_2Cu_2TeO_6$, was proposed [14–18]. Similar to $Na_3Cu_2SbO_6$, the Cu^{2+} ions ($S = \frac{1}{2}$) in $Na_2Cu_2TeO_6$ form a distorted honeycomb lattice in the *ab* plane, which are separated by the Na^+ layers along the *c* axis (see Fig. 1). Magnetic susceptibility measurements on a powder sample of $Na_2Cu_2TeO_6$ revealed a spin gap $\Delta \sim 127$ K [14], which has been attributed to strong AF couplings J_1 in the density functional theory (DFT) calculations [14,16–18]. However, controversy remains as to the sign of the intrachain coupling J_2: Magnetic susceptibility data can be fitted equally well by the FM or AF J_2 model [15], and this ambiguity is not resolved by contradictory DFT results that support either AF [14,16] or FM [17,18] J_2 couplings. The magnitude of J_3 also remains

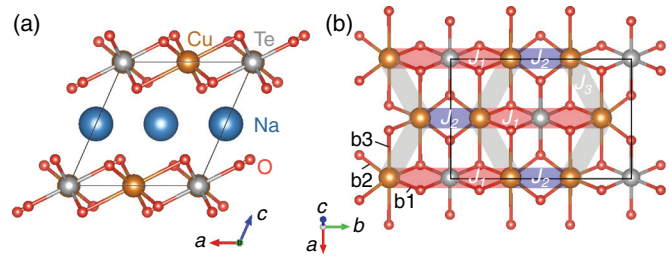

FIG. 1. (a), (b) Crystal structure of $Na_2Cu_2TeO_6$ viewed along the (a) *b* and (b) c^* axes with the Cu^{2+} ions forming chains along the *b* axis. The size of the unit cell is indicated by black lines. The Cu^{2+} spins are coupled through alternating J_1 (red) and J_2 (blue) interactions along the chain and J_3 interactions (gray) between the chains. Cu-O bonds of different lengths are indicated in the CuO_6 octahedron at the left bottom corner of (b), with $b1 = 1.978(1)$ Å, $b2 = 1.999(1)$ Å, and $b3 = 2.533(1)$ Å.

to be determined, as comparable J_2 and J_3 couplings might invalidate a spin chain scenario.

To establish whether $Na_2Cu_2TeO_6$ represents a rare realization of the alternating AF-FM spin chains, here we perform inelastic neutron scattering (INS) experiments on a single-crystal sample of $Na_2Cu_2TeO_6$ to determine the exchange coupling strengths. We confirm the spin gap originates from the dominant AF coupling J_1 (22.8 meV), and the interchain coupling J_3 is found to be much weaker (1.3 meV). Most importantly, we reveal the intrachain coupling J_2 to be FM with a strength (−8.7 meV) that is much higher than J_3, thus establishing $Na_2Cu_2TeO_6$ as a weakly coupled alternating AF-FM chain compound. Through the DFT calculations, the alternating signs of the interchain couplings can be attributed to their different exchange paths.

Experimental details. Polycrystalline $Na_2Cu_2TeO_6$ was utilized as a source material for crystal growth in a flux based on TeO_2 and Na_2CO_3. Details for the polycrystal synthesis and characterization can be found in the Supplemental Material [19]. Powders of these materials in a ratio of $2(Na_2Cu_2TeO_6):1(Na_2CO_3):4(TeO_2)$ were mixed and loaded into a Pt crucible that was covered with a Pt lid. The crucible was heated rapidly to 900 °C where the melt was homogenized for 12 h in air. The furnace was then cooled at 2 °C/h to 500 °C at which point it was turned off to cool. The translucent green crystals were recovered by boiling the product-filled crucible in a hot aqueous solution of potassium hydroxide, followed by additional rinsing in de-ionized water.

INS experiments on $Na_2Cu_2TeO_6$ were performed on the fine-resolution Fermi chopper spectrometer SEQUOIA at the Spallation Neutron Source (SNS) of the ORNL. A single crystal (mass ∼140 mg) was aligned with the (001) vector vertical. A closed cycle refrigerator (CCR) was employed to reach temperatures T down to 5 K. The incident neutron energy was $E_i = 60$ meV, and Fermi chopper frequencies of 180 and 420 Hz were selected in the high-intensity and high-resolution modes, respectively. Data were acquired by rotating the sample in 1° steps, covering a total range of 200° at 5 K and 100° at higher temperatures. Data reductions and projections were performed using MANTID [20] and HORACE software [21].

First-principles calculations using the projector augmented-wave (PAW) method were performed based on the DFT as implemented in the Vienna *ab initio* simulation package (VASP) code [22–24]. The generalized gradient approximation (GGA) and the revised Perdew-Burke-Ernzerhof (PBEsol) function were used to treat the electron exchange-correlation potential [25,26]. Based on the *ab initio* ground-state wave function, the Cu-site centered Wannier functions (WFs) with orbital $d_{x^2-y^2}$ were constructed using the WANNIER90 code [27,28].

Results. As shown in Fig. 1(a), the large separation of $c = 5.92$ Å between the honeycomb layers indicates likely negligible interlayer couplings. This is immediately confirmed in our single-crystal INS experiment. Figure 2(a) plots a representative slice of the measured spectrum along the Q_l direction that is perpendicular to the *ab* plane. A single excitation mode is observed at ∼18 meV, which is flat within the instrument resolution (1.6 meV at the elastic line). In contrast, strong dispersions in the energy range of $E = [17, 28]$ meV

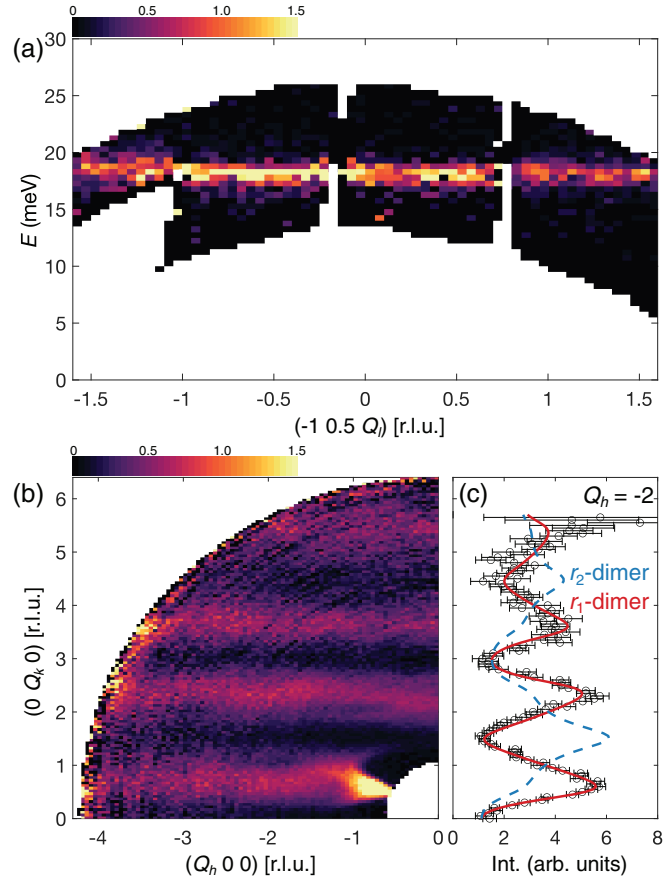

FIG. 2. (a) Scattering intensity of $Na_2Cu_2TeO_6$ measured along $(-1\ 0.5\ Q_l)$ at $T = 5$ K with integration widths of $\Delta Q_h = 0.2$ and $\Delta Q_k = 0.1$. Measurements were performed in the high-resolution configuration. (b) Intensity map in the $(Q_h\ Q_k\ 0)$ plane integrated over ranges of [17, 28] meV in E and $[-2, 2]$ in Q_l. Measurements were performed in the high-intensity setup at $T = 5$ K. (c) Scattering intensity along Q_k integrated from the map in (b) over the range of $[-2.1, 1.9]$ in Q_h. The intensity can be described by the structure factor of the r_1-dimer model (red solid line) instead of the r_2-dimer model (blue dashed line), where $r_1 \approx 2b/3$ and $r_2 \approx b/3$ are the bond distances for J_1 and J_2, respectively.

are observed in the *ab* plane as summarized in Figs. 3(a)–3(d), thus confirming all the related couplings to be within the honeycomb layers.

The lack of dispersion out of the *ab* plane allows us to integrate data along Q_l for better statistics. Figure 2(b) plots the scattering intensity integrated in the range of Q_l in $[-2, 2]$ (r.l.u.) and E in [17, 28] meV. Along the Q_k direction, intensity is strongly modulated with a periodicity of ∼1.5 (r.l.u.). For dimer systems, it is established that intensity of the triplon excitations is modulated by the dimer structure factor $S(\boldsymbol{Q}) \propto [1 - \cos(\boldsymbol{Q} \cdot \boldsymbol{r})]$, where $\boldsymbol{r}$ is the vector that connects the two spin sites within the dimer [29–31]. Therefore, the modulation along Q_k indicates that dimers in $Na_2Cu_2TeO_6$ are forming along the b axis, and its periodicity tells the bond distance r within the dimers. As shown in Fig. 2(c), the model that assumes dimers forming over the J_1 bonds with a distance of $r_1 = 2b/3$ accurately describes the intensity modulation,

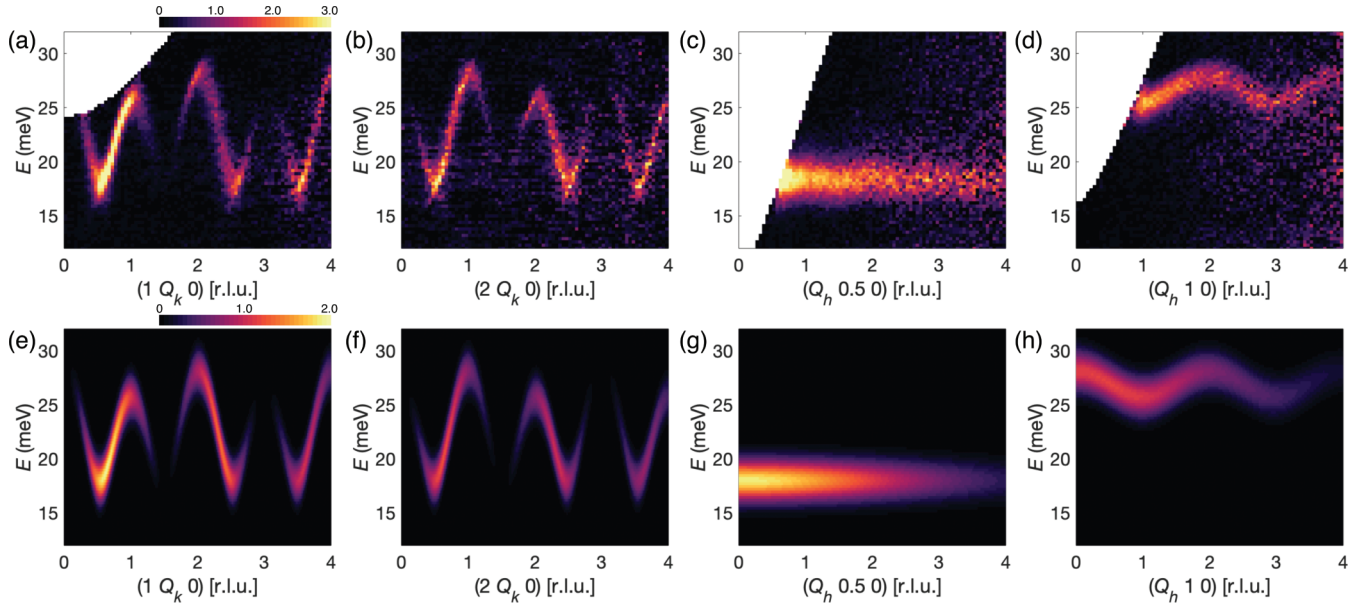

FIG. 3. (a)–(d) Intensity maps of $Na_2Cu_2TeO_6$ measured along (1 Q_k 0), (2 Q_k 0), (Q_h 0.5 0), and (Q_h 1 0) at $T = 5$ K using the high-intensity configuration. The integration widths are $\Delta Q_h = 0.1$, $\Delta Q_k = 0.1$, and $\Delta Q_l = 2$. (e)–(h) Intensity maps calculated through the random phase approximation with fitted coupling strengths $J_1 = 22.78(2)$ meV, $J_2 = -8.73(4)$ meV, and $J_3 = 1.34(3)$ meV. An instrumental energy resolution of 3.0 meV was convolved with the calculated spectrum. (a)–(d) and (e)–(h) are shown on the identical intensity scale, respectively.

thus confirming the J_1 couplings to be AF and dominant as proposed by the DFT calculations [15–18].

Figures 3(a)–3(d) summarize the dispersion along Q_h and Q_k in the *ab* plane. Along the chain direction (Q_k), the triplon band reaches its lowest energy of ∼18 meV at $Q_k = N + 1/2$ with integer N, indicating the FM character of the interdimer J_2 couplings [11,32]. Different from the conventional chain compounds, the top of the dispersion varies at successive integer Q_k positions, which might arise from the interchain couplings. As compared in Figs. 3(c) and 3(d), although the triplon band looks flat along (Q_h 0.5 0) at the bottom of the band, dispersion with a bandwidth of ∼3 meV is observed along (Q_h 1 0) at the top of the band, which suggests weak but non-negligible J_3 couplings.

The triplon dispersion in dimer systems can often be analyzed through the random phase approximation [29,33–36]. Under this approximation, the dispersion relation can be written as

$$\hbar\omega(\boldsymbol{Q}) = \sqrt{J_1^2 + J_1 \mathcal{J}(\boldsymbol{Q}) R(T)}, \tag{1}$$

where $R(T)$ describes the population difference between the singlet and triplet states [29,34] and for $Na_2Cu_2TeO_6$ can be approximated by 1 at $T = 5$ K due to the large excitation gap. $\mathcal{J}(\boldsymbol{Q})$ is the Fourier sum of interactions beyond the dimer exchange,

$$\mathcal{J}(\boldsymbol{Q}) = -J_2 \cos(2\pi Q_k) - 2J_3 \cos(\pi Q_h)\cos(\pi Q_k). \tag{2}$$

Experimental dispersion values were extracted from Gaussian fits to constant Q scans at 140 points throughout the measured reciprocal space volume, which were then fitted by the dispersion relation in Eq. (1). The fitted coupling strengths are $J_1 = 22.78(2)$ meV, $J_2 = -8.73(4)$ meV, and $J_3 = 1.34(3)$ meV. The calculated spectra are summarized in Figs. 3(e)–3(h) for comparison with the experimental data. The FM character of the J_2 couplings is thus unambiguously established, and the weakness of the interchain J_3 justifies the description of $Na_2Cu_2TeO_6$ as a weakly coupled alternating AF-FM chain compound.

In Haldane chains the existence of a spin gap is known to protect the spin entanglement [37]. $Na_2Cu_2TeO_6$ can serve as a model system to test that the same ideas are valid for alternating spin chains. In long-range ordered magnets, the excitation gap often decreases at higher T due to reduced ordering moments. As a contrast, the gap of Haldane chains increases with T due to the reduction in the coherent length and the consequent finite-size effect [38,39]. The E scans at $\boldsymbol{Q} = (1, 0.5, 0)$ shown in Fig. 4(a) indeed reveal an increased gap at elevated T. We parametrize the line shape using a Gaussian function that is independently fit at each temperature, and the value of Δ is the centroid of the Gaussian peak. As summarized in Fig. 4(b), in a large range below ∼150 K, the fitted gap size Δ and full width at half maximum (FWHM) Γ exhibit an activated behavior that is characteristic of Haldane chains [40,41],

$$\Delta(T) = \Delta_0 + \sqrt{\alpha T}\exp(-\Delta_0/T),$$
$$\Gamma(T) = \Gamma_0 + \gamma\exp(-\Delta_0/T), \tag{3}$$

where α, γ, and Γ_0 are fitting parameters, and Δ_0 is the gap size at 0 K and is fixed at 18.0 meV. The validity of the activated behavior further confirms the similarity between the $S = \frac{1}{2}$ alternating AF-FM chains and the integer-spin Haldane chains, thus revealing the robustness of the topological ground state against weak interchain couplings.

Discussion. The emergence of spin chains in $Na_2Cu_2TeO_6$ can be ascribed to the distortion of the honeycomb lattice. As shown in Fig. 1(b), the exchange paths of J_3 involve the longest Cu-O bonds *b*3 of the distorted octahedra. Therefore,

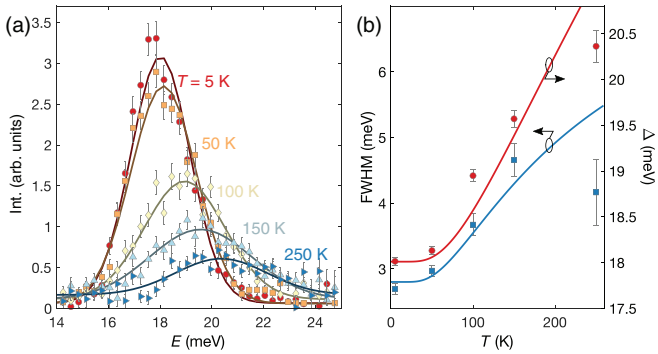

FIG. 4. (a) Energy dependence of the scattering intensity at (1 0.5 0) measured at $T = 5$ (circles), 50 (squares), 100 (diamonds), 150 (up-pointing triangles), and 250 (right-pointing triangles) K. Solid lines are Gaussian fits. (b) Temperature dependence of the fitted gap size Δ (circles, right axis) and full width at half maximum FWHM (squares, left axis). Solid lines are fits using the empirical formula in Eq. (3). The fitted parameters are $\alpha = 2.3(8)$ meV, $\gamma = 6(2)$ meV, and $\Gamma_0 = 2.8(2)$ meV. At low temperatures, the FWHM is close to the instrumental energy resolution.

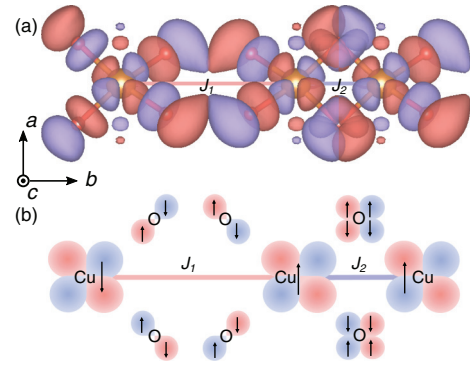

FIG. 5. (a) Wannier functions of the Cu $3d_{x^2-y^2}$ orbital, an antibonding combination of the Cu $3d_{x^2-y^2}$ and O $2p$ states, viewed along the c axis. Different colors represent the $+/-$ signs of the Wannier function. (b) Diagrams for the supersuperexchange and superexchange couplings between the nearest-neighbor Cu $3d_{x^2-y^2}$ orbitals via oxygen $2p$ ligands. For the J_1 path, the Cu-O$\cdots$O-Cu supersuperexchange leads to the AF alignment of the nearest-neighbor Cu ions. For the J_2 path, Cu-O-Cu superexchange with a bonding angle of 90° results in a FM exchange between the nearest-neighbor Cu ions.

the J_3 couplings are expected to be weak as the unoccupied Cu $3d_{x^2-y^2}$ orbitals disfavor the elongated bond direction, which reduces the electron hopping between the chains.

The sign of the interchain couplings J_2 is more subtle, and different scenarios exist in the previous DFT calculations [14,16–18]. As summarized in the Supplemental Material, our DFT calculations confirm the alternating FM and AF intrachain couplings, in agreement with the experiment. The contrasting J_1 and J_2 couplings can be understood through the Wannier functions (WFs) as plotted in Fig. 5(a). Due to the contributions from the O $2p$ states, the WFs overlap directly over the J_1 paths but are almost orthogonal over the J_2 path. Therefore, the J_1 path, in spite of its longer distance, develops a stronger coupling than that over the J_2 path. Based on the WFs, the signs of the couplings can be understood through the Goodenough-Kanamori-Anderson rules [42–45] as shown in Fig. 5(b). For the J_1 couplings, the Cu-O$\cdots$O-Cu supersuperexchange leads to an AF interaction between the Cu^{2+} spins, while for the J_2 couplings, the interaction become FM as the angle of $\angle$ Cu-O-Cu is close to $\sim$90°, which means a pair of orthogonal O $2p$ orbitals with parallel spins are involved in the virtual electron hopping.

Conclusions. Neutron scattering experiments have been performed on the honeycomb lattice compound $Na_2Cu_2TeO_6$ to study its spin correlations. A triplon excitation mode was observed, which exhibits strong dispersion along the chain but weak dispersion perpendicular to the chain. Under the random phase approximation, the intrachain couplings were found to be alternating AF and FM, and a weak interchain coupling was also established. The emergence of spin chains in $Na_2Cu_2TeO_6$ was ascribed to the distortion of the honeycomb lattice, and the alternating intrachain couplings were understood through the DFT calculations. Our works establish the existence of weakly coupled alternating AF-FM spin-$\frac{1}{2}$ chains in $Na_2Cu_2TeO_6$ and reveal a robust gapped ground state that is similar to that of the integer-spin Haldane chains.

Acknowledgments. We acknowledge helpful discussions with Jyong-Hao Chen, Tong Chen, and Tao Hong. This work was supported by the U.S. Department of Energy, Office of Science, Basic Energy Sciences, Materials Sciences and Engineering Division. This research used resources at the Spallation Neutron Source (SNS), a DOE Office of Science User Facility operated by the Oak Ridge National Laboratory (ORNL). ORNL is managed by UT-Battelle, LLC, under Contract No. DE-AC05-00OR22725 with the U.S. Department of Energy. The U.S. Government retains, and the publisher, by accepting the article for publication, acknowledges that the U.S. Government retains a nonexclusive, paid-up, irrevocable, worldwide license to publish or reproduce the published form of this manuscript, or allow others to do so, for U.S. Government purposes. The Department of Energy will provide public access to these results of federally sponsored research in accordance with the DOE Public Access Plan [51].

[1] K. Hida, Ground-state phase diagram of the spin-1/2 ferromagnetic-antiferromagnetic alternating heisenberg chain with anisotropy, Phys. Rev. B **46**, 8268 (1992).

[2] K. Hida, Excitation spectrum of the spin-1/2 ferromagnetic-antiferromagnetic alternating Heisenberg chain, J. Phys. Soc. Jpn. **63**, 2514 (1994).

[3] H. Bethe, Zur Theorie der Metalle. I. Eigenwerte und Eigenfunktionen der linearen Atomkette, Z. Phys. **71**, 205 (1931).

[4] F. D. M. Haldane, Nonlinear Field Theory of Large-Spin Heisenberg Antiferromagnets: Semiclassically Quantized Solitons of the One-Dimensional Easy-Axis Néel State, Phys. Rev. Lett. **50**, 1153 (1983).

[5] I. Affleck, T. Kennedy, E. H. Lieb, and H. Tasaki, Rigorous Results on Valence-Bond Ground States in Antiferromagnets, Phys. Rev. Lett. **59**, 799 (1987).

[6] K. Hida, Crossover between the Haldane-gap phase and the dimer phase in the spin-1/2 alternating Heisenberg chain, Phys. Rev. B **45**, 2207 (1992).

[7] M. Kohmoto and H. Tasaki, Hidden $Z_2 \times Z_2$ symmetry breaking and the Haldane phase in the $S = 1/2$ quantum spin chain with bond alternation, Phys. Rev. B **46**, 3486 (1992).

[8] F. Pollmann, A. M. Turner, E. Berg, and M. Oshikawa, Entanglement spectrum of a topological phase in one dimension, Phys. Rev. B **81**, 064439 (2010).

[9] A. Miyake, Quantum Computation on the Edge of a Symmetry-Protected Topological Order, Phys. Rev. Lett. **105**, 040501 (2010).

[10] K. Kodama, H. Harashina, H. Sasaki, M. Kato, M. Sato, K. Kakurai, and M. Nishi, Neutron scattering study on the quasi-one-dimensional spin-gap system $CuNb_2O_6$, J. Phys. Soc. Jpn. **68**, 237 (1999).

[11] M. B. Stone, W. Tian, M. D. Lumsden, G. E. Granroth, D. Mandrus, J.-H. Chung, N. Harrison, and S. E. Nagler, Quantum Spin Correlations in an Organometallic Alternating-Sign Chain, Phys. Rev. Lett. **99**, 087204 (2007).

[12] Y. Miura, Y. Yasui, T. Moyoshi, M. Sato, and K. Kakurai, Magnetic excitations of spin-gap system $Na_3Cu_2SbO_6$ with distorted honeycomb structure, J. Phys. Soc. Jpn. **77**, 104709 (2008).

[13] E. S. Klyushina, A. T. M. N. Islam, J. T. Park, E. A. Goremychkin, E. Wheeler, B. Klemke, and B. Lake, $S = 1/2$ dimerized antiferromagnetic-ferromagnetic quantum spin chain $BaCu_2V_2O_8$, Phys. Rev. B **98**, 104413 (2018).

[14] J. Xu, A. Assoud, N. Soheilnia, S. Derakhshan, H. L. Cuthbert, J. E. Greedan, M. H. Whangbo, and H. Kleinke, Synthesis, structure, and magnetic properties of the layered copper(II) oxide $Na_2Cu_2TeO_6$, Inorg. Chem. **44**, 5042 (2005).

[15] Y. Miura, R. Hirai, Y. Kobayashi, and M. Sato, Spin-gap behavior of $Na_3Cu_2SbO_6$ with distorted honeycomb structure, J. Phys. Soc. Jpn. **75**, 084707 (2006).

[16] S. Derakhshan, H. L. Cuthbert, J. E. Greedan, B. Rahaman, and T. Saha-Dasgupta, Electronic structures and low-dimensional magnetic properties of the ordered rocksalt oxides $Na_3Cu_2SbO_6$ and $Na_2Cu_2TeO_6$, Phys. Rev. B **76**, 104403 (2007).

[17] H.-J. Koo and M.-H. Whangbo, Analysis of the spin lattice model for the spin-gapped layered compounds $Na_3Cu_2SbO_6$ and $Na_2Cu_2TeO_6$ on the basis of electronic structure calculations, Inorg. Chem. **47**, 128 (2008).

[18] M. Schmitt, O. Janson, S. Golbs, M. Schmidt, W. Schnelle, J. Richter, and H. Rosner, Microscopic magnetic modeling for the $Na_3Cu_2SbO_6$ and $Na_2Cu_2TeO_6$, Phys. Rev. B **89**, 174403 (2014).

[19] See Supplemental Material at http://link.aps.org/supplemental/10.1103/PhysRevB.102.220402 for details on the preparation and characterizations of the powder sample and the DFT calculations, which includes Refs. [46–50].

[20] O. Arnold, J. Bilheux, J. Borreguero, A. Buts, S. Campbell, L. Chapon, M. Doucet, N. Draper, R. Ferraz Leal, M. Gigg, V. Lynch, A. Markvardsen, D. Mikkelson, R. Mikkelson, R. Miller, K. Palmen, P. Parker, G. Passos, T. Perring, P. Peterson *et al.*, Mantid—Data analysis and visualization package for neutron scattering and μSR experiments, Nucl. Instrum. Methods Phys. Res., Sect. A **764**, 156 (2014).

[21] R. Ewings, A. Buts, M. Le, J. van Duijn, I. Bustinduy, and T. Perring, Horace: Software for the analysis of data from single crystal spectroscopy experiments at time-of-flight neutron instruments, Nucl. Instrum. Methods Phys. Res., Sect. A **834**, 132 (2016).

[22] G. Kresse and J. Furthmüller, Efficient iterative schemes for *ab initio* total-energy calculations using a plane-wave basis set, Phys. Rev. B **54**, 11169 (1996).

[23] G. Kresse and D. Joubert, From ultrasoft pseudopotentials to the projector augmented-wave method, Phys. Rev. B **59**, 1758 (1999).

[24] P. E. Blöchl, Projector augmented-wave method, Phys. Rev. B **50**, 17953 (1994).

[25] J. P. Perdew, K. Burke, and M. Ernzerhof, Generalized Gradient Approximation Made Simple, Phys. Rev. Lett. **77**, 3865 (1996).

[26] J. P. Perdew, A. Ruzsinszky, G. I. Csonka, O. A. Vydrov, G. E. Scuseria, L. A. Constantin, X. Zhou, and K. Burke, Restoring the Density-Gradient Expansion for Exchange in Solids and Surfaces, Phys. Rev. Lett. **100**, 136406 (2008).

[27] N. Marzari and D. Vanderbilt, Maximally localized generalized Wannier functions for composite energy bands, Phys. Rev. B **56**, 12847 (1997).

[28] A. A. Mostofi, J. R. Yates, Y.-S. Lee, I. Souza, D. Vanderbilt, and N. Marzari, WANNIER90: A tool for obtaining maximally-localised Wannier functions, Comput. Phys. Commun. **178**, 685 (2008).

[29] B. Leuenberger, A. Stebler, H. U. Güdel, A. Furrer, R. Feile, and J. K. Kjems, Spin dynamics of an isotropic singlet-ground-state antiferromagnet with alternating strong and weak interactions: An inelastic-neutron-scattering study of the dimer compound $Cs_3Cr_2Br_9$, Phys. Rev. B **30**, 6300 (1984).

[30] G. Xu, C. Broholm, D. H. Reich, and M. A. Adams, Triplet Waves in a Quantum Spin Liquid, Phys. Rev. Lett. **84**, 4465 (2000).

[31] N. Cavadini, G. Heigold, W. Henggeler, A. Furrer, H.-U. Güdel, K. Krämer, and H. Mutka, Magnetic excitations in the quantum spin system $TlCuCl_3$, Phys. Rev. B **63**, 172414 (2001).

[32] D. A. Tennant, C. Broholm, D. H. Reich, S. E. Nagler, G. E. Granroth, T. Barnes, K. Damle, G. Xu, Y. Chen, and B. C. Sales, Neutron scattering study of two-magnon states in the quantum magnet copper nitrate, Phys. Rev. B **67**, 054414 (2003).

[33] S. B. Haley and P. Erdös, Standard-basis operator method in the Green's-function technique of many-body systems with an application to ferromagnetism, Phys. Rev. B **5**, 1106 (1972).

[34] M. B. Stone, M. D. Lumsden, S. Chang, E. C. Samulon, C. D. Batista, and I. R. Fisher, Singlet-Triplet Dispersion Reveals Additional Frustration in the Triangular-Lattice Dimer $Ba_3Mn_2O_8$, Phys. Rev. Lett. **100**, 237201 (2008).

[35] M. B. Stone, M. D. Lumsden, Y. Qiu, E. C. Samulon, C. D. Batista, and I. R. Fisher, Dispersive magnetic excitations in the $S = 1$ antiferromagnet $Ba_3Mn_2O_8$, Phys. Rev. B **77**, 134406 (2008).

[36] S. Allenspach, A. Biffin, U. Stuhr, G. S. Tucker, S. Ohira-Kawamura, M. Kofu, D. J. Voneshen, M. Boehm, B. Normand, N. Laflorencie, F. Mila, and C. Rüegg, Multiple Magnetic Bi-

layers and Unconventional Criticality without Frustration in $BaCuSi_2O_6$, Phys. Rev. Lett. **124**, 177205 (2020).

[37] K. Wierschem and P. Sengupta, Characterizing the Haldane phase in quasi-one-dimensional spin-1 Heisenberg antiferromagnets, Mod. Phys. Lett. B **28**, 1430017 (2014).

[38] T. Jolicœur and O. Golinelli, σ model study of Haldane-gap antiferromagnets, Phys. Rev. B **50**, 9265 (1994).

[39] M. P. Nightingale and H. W. J. Blöte, Gap of the linear spin-1 Heisenberg antiferromagnet: A Monte Carlo calculation, Phys. Rev. B **33**, 659 (1986).

[40] A. Zheludev, S. E. Nagler, S. M. Shapiro, L. K. Chou, D. R. Talham, and M. W. Meisel, Spin dynamics in the linear-chain $S = 1$ antiferromagnet $Ni(C_3H_{10}N_2)_2N_3(ClO_4)$, Phys. Rev. B **53**, 15004 (1996).

[41] A. K. Bera, B. Lake, A. T. M. N. Islam, and A. Schneidewind, Critical properties of coupled anisotropic Haldane spin chains in a magnetic field, Phys. Rev. B **92**, 060412(R) (2015).

[42] P. W. Anderson, Antiferromagnetism. Theory of superexchange interaction, Phys. Rev. **79**, 350 (1950).

[43] J. B. Goodenough, Theory of the role of covalence in the perovskite-type manganites [La,M(II)]MnO_3, Phys. Rev. **100**, 564 (1955).

[44] J. B. Goodenough, An interpretation of the magnetic properties of the perovskite-type mixed crystals $La_{1-x}Sr_xCoO_{3-\lambda}$, J. Phys. Chem. Solids **6**, 287 (1958).

[45] A. S. Moskvin, N. S. Ovanesyan, and V. A. Trukhtanov, Angular dependence of the superexchange interaction Fe^{3+}-O^{2-}-Cr^{3+}, Hyperfine Interact. **1**, 265 (1975).

[46] J. Rodriguez-Carvajal, Recent advances in magnetic structure determination by neutron powder diffraction, Physica B: Condens. Matter **192**, 55 (1993).

[47] Z. Wang, N. Qureshi, S. Yasin, A. Mukhin, E. Ressouche, S. Zherlitsyn, Y. Skourski, J. Geshev, V. Ivanov, M. Gospodinov, and V. Skumryev, Magnetoelectric effect and phase transitions in CuO in external magnetic fields, Nat. Commun. **7**, 10295 (2016).

[48] S. L. Dudarev, G. A. Botton, S. Y. Savrasov, C. J. Humphreys, and A. P. Sutton, Electron-energy-loss spectra and the structural stability of nickel oxide: An LSDA+U study, Phys. Rev. B **57**, 1505 (1998).

[49] H. Jeschke, I. Opahle, H. Kandpal, R. Valentí, H. Das, T. Saha-Dasgupta, O. Janson, H. Rosner, A. Brühl, B. Wolf, M. Lang, J. Richter, S. Hu, X. Wang, R. Peters, T. Pruschke, and A. Honecker, Multistep Approach to Microscopic Models for Frustrated Quantum Magnets: The Case of the Natural Mineral Azurite, Phys. Rev. Lett. **106**, 217201 (2011).

[50] O. Janson, I. Rousochatzakis, A. A. Tsirlin, M. Belesi, A. A. Leonov, U. K. Rößler, J. van den Brink, and H. Rosner, The quantum nature of skyrmions and half-skyrmions in Cu_2OSeO_3, Nat. Commun. **5**, 5376 (2014).

[51] http://energy.gov/downloads/doe-public-access-plan.